KOPSKY, V. (1979). *Acta Cryst.* A**35**, 83–95.
LANDAU, L. & LIFSHITZ, E. (1959). *Theory of Elasticity*, 1st ed. London/Paris: Pergamon.
LAX, M. (1974). *Symmetry Principle in Solid State and Molecular Physics*. New York: John Wiley.
LIN, S.-Y., WANG, X.-M., LU, L., ZHANG, D.-L., HE, L. X. & KUO, K. H. (1990). *Phys. Rev.* B**41**, 9625–9627.
NYE, J. F. (1985). *Physical Properties of Crystals*. Oxford: Clarendon Press.
RAMA MOHANA RAO, K. & HEMAGIRI RAO (1992). *J. Phys. Condens. Matter*, **4**, 5997–6008.
RAMA MOHANA RAO, K. & HEMAGIRI RAO (1993). *J. Phys. Condens. Matter*, **5**, 5513–5524.
REYNOLDS, G. A. M., GOLDING, B., KORTAN, A. R. & PARSEY, J. M. JR. (1990). *Phys. Rev. B*, **41**, 1194–1195.
RIPAMONTI, C. (1987). *J. Phys. (Paris)*, **48**, 893–895.
SCHECHTMAN, D., BLECH, I., GRATIAS, D. & CAHN, J. W. (1984). *Phys. Rev. Lett.* **53**, 1952–1953.
VANDERWAL, J. J., ZHAO, P. & WALTON, D. (1992). *Phys. Rev. B*, **46**, 501–502.
WANG, Y.-P., ZHANG, D.-L. & CHEN, L. F. (1993). *Phys. Rev. B*, **48**, 10542–10545.
ZHANG, D.-L., CAO, X.-C., WANG, Y.-P., LU, L., WANG, X.-M., MA, X. L. & KUO, K. H. (1991). *Phys. Rev. Lett.* **66**, 2778–2781.
ZHANG, D.-L., LU, L., WANG, X.-M., LIN, S.-Y., HE, L. X. & KUO, K. H., (1990). *Phys. Rev. B*, **41**, 8557–8559.

Acta Cryst. (1995). A**51**, 163–171

X-ray Diffraction Profiles in Strained Crystals Undergoing Ultrasonic Excitation. The Laue Case

BY E. ZOLOTOYABKO AND B. SANDER

Department of Materials Engineering, Technion-Israel Institute of Technology, Haifa 32000, *Israel*

(*Received* 23 *May* 1994; *accepted* 4 *August* 1994)

Abstract

A new approach for the calculation of diffraction profiles in strained crystals is developed, based on the visual concepts of the dispersion surface and Poynting vectors. By this approach, analytical expressions have been obtained for diffraction profiles for the case of a constant strain gradient without, as well as with, ultrasonic excitation. Calculations of acoustically induced modifications in diffraction spectra explain in detail the anomalous dependence of integrated intensity on ultrasound amplitude, a dependence that was recently found in the Laue scattering geometry.

1. Introduction

The sensitivity of X-ray diffraction to static strain fields in single crystals is traditionally used to study lattice distortions related to crystal defects. Recently, attention has been given to X-ray diffraction under dynamic deformations created by high-frequency ultrasound (US) (Kohler, Mohling & Peibst, 1974; Entin, 1977, 1979; Entin & Assur, 1981; Chapman, Colella & Bray, 1983) as a result of the new possibilities of measuring weak US fields (Cerva & Graff, 1984; Andreev, Ponomarev & Smolin, 1988; Zolotoyabko, Panov & Schvarkov, 1993; Zolotoyabko, Jacobsohn, Shechtman, Kantor & Salzman, 1993) and of acoustically controlling X-ray beams in space and time (Kikuta, Takahashi & Nakatani, 1984; Kocharyan, Sukiasyan, Megrabyan & Sarkisyan, 1989; Roshchupkin, Brunel, Bergevin & Erko, 1992). Moreover, it turns out that diffraction processes in the presence of combined static and dynamic deformation fields are of great interest, because of the high sensitivity of US-induced diffraction effects to small intrinsic strains in the samples. Few works (Entin, Khrupa & Datsenko, 1990; Khrupa, Entin & Datsenko, 1991; Zolotoyabko, Polikarpov, Panov & Schvarkov, 1992; Raranskii, Fodchuk, Novikov & Korovyanko, 1993) have been devoted to the development of new methods for the characterization of the structural quality of semiconductor crystals using the high sensitivity mentioned. The application of these methods is limited, however, by insufficient knowledge about diffraction phenomena in complex static and dynamic deformation fields in real crystals with defects and subsequent difficulties related to the interpretation of experimental data. A comprehensive analysis can be performed for crystals homogeneously bent by a constant strain gradient (Iolin, 1987; Iolin, Raitman, Kuvaldin & Zolotoyabko, 1988; Zolotoyabko & Panov, 1992; Chukhovskii, Nosik & Iolin, 1993). Even in this model case interesting effects such as a new type of *Pendellösung* fringe (Zolotoyabko & Panov, 1992) and the anomalous behaviour of the integrated diffraction intensity S (Iolin, Raitman, Kuvaldin & Zolotoyabko, 1988; Zolotoyabko & Panov, 1992) were observed under US excitation. These effects shed some light on the mechanisms of X-ray–acoustic interaction in strained crystals. For example, the anomalous behaviour of S consists of a substantial decrease (by up to 50%) of S

under small US amplitudes w ($Hw < 1$, where H is the magnitude of the reciprocal-lattice vector) (see Fig. 1). The opposite (normal) behaviour of S occurs in an undistorted crystal where an $S(w)$ growth is observed (see Fig. 1), owing to the formation of satellites (caused by X-ray scattering on an acoustic superlattice). Actually, in a distorted crystal, an angular interval $\Delta\Theta \simeq \varepsilon$ in the diffraction profile, determined from the intrinsic strain ε, can be considered as already 'excited' by the strain gradient. Thus, in the angular range ε, the formation of satellites is suppressed, preventing an increase in S. Moreover, as shown by Iolin (1987) and Iolin, Raitman, Kuvaldin & Zolotoyabko (1988), the US-stimulated interbranch scattering processes lead to a decrease in diffraction intensity, as if 'restoring' the lattice to its perfect state. This pronounced difference in the $S(w)$ dependence in perfect and strained crystals (see Fig. 1) is of great importance because it can be used for small strain determination. As an outcome of this behaviour of integrated diffraction intensity, the following dynamics of diffraction profiles are proposed (Zolotoyabko, Sander, Komem & Kantor, 1994). When the US-induced dynamic strain $\delta = 2|\mathbf{k}|w$ (where $\mathbf{k}$ is the US wave vector) exceeds the static strain ε, a broadening of the diffraction profile is expected, as a result of satellite formation, that provides an increase in $S(w)$. In order to explain the experimentally obtained decrease in S, it is assumed that, in the opposite limit, $\delta < \varepsilon$, interbranch scattering processes can lead to a narrowing of the diffraction profile. In fact, the narrowing effect at small US amplitudes was observed in the Bragg scattering geometry (Zolotoyabko, Sander, Komem & Kantor, 1994) and was found to be a promising tool for a high-sensitivity strain-measurement method in semiconductor structures (Zolotoyabko, Sander, Komem & Kantor, 1993). Because of this practical significance, it is necessary to develop a detailed model for the transformation of diffraction profiles under US influence in order to achieve a deeper understanding of the phenomena discussed and to get a quantitative basis for a new strain-analysis method.

Here the corresponding theory is developed for the simpler Laue case, where the difficulties related to the existence of imaginary wave vectors (Bonse, 1964) are not present.

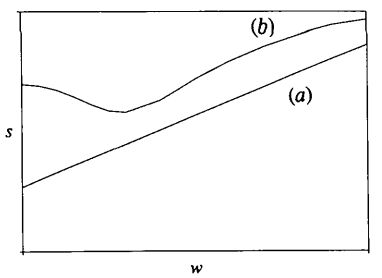

Fig. 1. Schematic plot of integrated diffraction intensity, S, as a function of ultrasound amplitude w: (*a*) in a perfect crystal; (*b*) in a strained crystal.

2. X-ray diffraction profiles without ultrasound

X-ray diffraction in elastically strained crystals in the Laue geometry without US has been considered many times, starting from the classical works of Penning & Polder (1961), Penning (1966) and Kato (1963, 1964), based on the concept of geometrical optics. These theories were visual and provided a clear description of diffraction phenomena, following the movement of tie points in momentum space along the dispersion surface. A detailed review of this approach can be found in an article by Hart (1980). Further progress was achieved with the solution of the Takagi equations in real space (Takagi, 1962, 1969), which provided a universal approach to dealing with slowly varing deformation fields. Nevertheless, the analytical solution of Takagi equations even in the case of homogeneous bending is very complicated (Chukhovskii & Petrashen, 1977). The introduction of US deformation increases the mathematical complexity, and reasonable expressions for the integrated diffraction intensity (Chukhovskii, Nosik & Iolin, 1993) could be obtained only in some asymptotic regimes, without any visualization of the variations in diffraction profiles. A completely different approach to the description of diffraction phenomena in strained crystals (including crystals under US excitation) is developed herein, based on the visual concepts of the dispersion surface and Poynting vectors.

Consider a standard dispersion surface (symmetrical Laue case) in the two-beam approximation (see Fig. 2) for a perfect nonabsorbing crystal. The shape of the dispersion surface is described by an equation joining the variations of the X-ray wave vector inside the crystal along (δk_x) and perpendicular to (δk_z) the entrance crystal surface (Pinsker, 1978):

$$(\delta k_z)^2 = (\delta k_x)^2 \tan^2 \Theta_B + (\Delta K_o/2)^2 \qquad (1)$$

where Θ_B is the Bragg angle and $\Delta K_o = 2\pi/\tau$ is the characteristic gap inversely proportional to the extinction length τ. By the introduction of dimensionless parameters,

$$q = 2\delta k_z/\Delta K_o \quad \text{and} \quad p = 2\delta k_x \tan\Theta_B/\Delta K_o, \qquad (2)$$

a simple relation between q and p,

$$q = \pm(1 + p^2)^{1/2}, \qquad (3)$$

is obtained for the upper (+) and lower (−) branches of the hyperbolic dispersion surface. At any given angle of incidence Θ, which is defined by parameter p as

$$\Theta - \Theta_B = \Delta\Theta = \Delta K_o p/H, \qquad (4)$$

two wave fields are excited (corresponding to the tie points $i = 1, 2$; see Fig. 2) with amplitudes of transmitted

(X_i) and diffracted (Y_i) components (Pinsker, 1978)

$$|X_1| = A[(1 + p^2)^{1/2} - p]/2(1 + p^2)^{1/2},$$
$$|X_2| = A[(1 + p^2)^{1/2} + p]/2(1 + p^2)^{1/2} \quad (5)$$

and

$$|Y_1| = |Y_2| = A/2(1 + p^2)^{1/2},$$

where A is the amplitude of the incident wave on the entrance crystal surface. It should be noted that, for further calculations of the averaged (over interference fringes) diffraction profiles, the phases of X_i and Y_i are insignificant. For a perfect crystal, the averaged diffraction intensity $I_o(p)$ at a given p value (diffraction profile) is simply calculated by means of (5)

$$I_o(p) = |Y_1|^2 + |Y_2|^2 = A^2/2(1 + p^2). \quad (6)$$

From (5), it is immediately checked that the sum

$$|X_1|^2 + |X_2|^2 + |Y_1|^2 + |Y_2|^2 = A^2 \quad (7)$$

is a constant independent of p, in accordance with the energy-conservation law. The values $|X_i|^2$ and $|Y_i|^2$ are the components of the corresponding Poynting vectors

$$\mathbf{P}_i = (c/8\pi)(|X_i|^2\mathbf{s}_0 + |Y_i|^2\mathbf{s}_H) \quad (8)$$

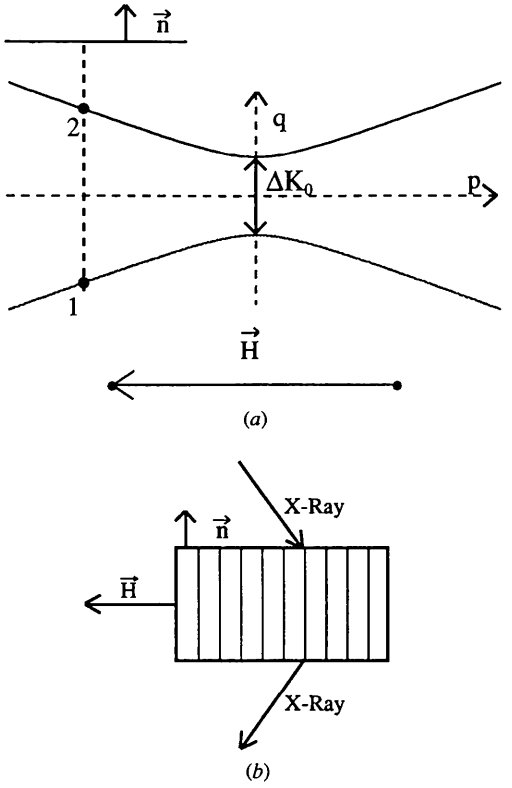

Fig. 2. (*a*) X-ray dispersion surface with stationary tie points 1 and 2 for a perfect crystal in the symmetrical Laue scattering geometry [(*b*)]. **n** is the normal to the entrance crystal surface.

(c is the velocity of light, $\mathbf{s}_0$ and $\mathbf{s}_H$ are the unit vectors in the directions of the transmitted and diffracted X-rays, respectively), describing the density of the energy flux in each wave field ($i = 1, 2$) (Pinsker, 1978).

Such energy considerations were used to calculate the diffraction intensity by a new method, which allows generalization for distorted crystals without, as well as with, US exitation. The diffraction process is divided into two parts: excitation of a given wave field (initial state p) on the entrance crystal surface, with an intensity

$$E_i(p) = |X_i(p)|^2 + |Y_i(p)|^2, \quad i = 1, 2, \quad (9)$$

and its subsequent transformation to the diffraction component measured at the exit crystal surface (final state p'), which is described by the factor

$$\xi_j(p') = |Y_j(p')|^2/[|X_j(p')|^2 + |Y_j(p')|^2], \quad j = 1, 2. \quad (10)$$

Both wave fields contribute to the diffraction profile $I(p)$. Moreover, owing to interbranch scattering processes, the initial and final states can be found, in principle, on different branches of the dispersion surface. Thus,

$$I(p) = \alpha_{ij}E_i(p)\xi_j(p') = \alpha_{ij}L_{ij}, \quad (11)$$

where the probabilities α_{ij} depend on the specific scattering mechanism.

In a perfect crystal, the initial and final states correspond to the same tie point on the dispersion surface, *i.e.* $p = p'$. The tie points are stationary because the diffraction conditions are identical at every point along the X-ray trajectory inside the crystal. In addition, the diffraction process takes place without branch mixing ($\alpha_{11} = \alpha_{22} = 1$; $\alpha_{12} = \alpha_{21} = 0$) and so the diffraction intensity is given by

$$I_0(p) = E_1(p)\xi_1(p) + E_2(p)\xi_2(p). \quad (12)$$

Substitution of (9) and (10) into (12) under the condition $p = p'$ gives, again, (6). Nontrivial results are obtained for an elastically bent crystal. In this case, tie points will move along the branches of the dispersion surface (see Fig. 3) and this movement reflects a modification in diffraction conditions while X-rays penetrate the crystal. The direction and the range of this movement is determined by the sign and magnitude of the strain gradient **b**, as well as by the crystal thickness T (Penning, 1966). In fact, for a cylindrical bending, $|\mathbf{b}| = R^{-1}$ (where R is the radius of curvature). Therefore, the relation between the deviation angle of atomic planes (see Fig. 3) and the thickness T is

$$\Delta\Theta_d = T/R = |\mathbf{b}|T. \quad (13)$$

The deviation angle (13) corresponds to a difference in momentum space between the initial, p, and final, p',

states of X-ray quanta:

$$p' = p + N, \tag{14}$$

with a shift value

$$N = |\mathbf{b}|TH/\Delta K_o \tag{15}$$

obtained using (4) and (13). The presence of a strain gradient gives rise to interbranch scattering processes (Chukhovskii, 1980), which are described in our scheme by contributions L_{ij} with $i \neq j$. Now, by means of (5), (9), (10) and (14), all the terms $L_{ij} = E_i(p)\xi_j(p')$ that contribute to the diffraction intensity can be calculated:

$$\begin{aligned}
L_{11} &= (A^2/4)\{1 - [p/(1+p^2)^{1/2}]\} \\
&\quad \times (1 + \{(p+N)/[1+(p+N)^2]^{1/2}\}) \\
L_{22} &= (A^2/4)\{1 + [p/(1+p^2)^{1/2}]\} \\
&\quad \times (1 - \{(p+N)/[1+(p+N)^2]^{1/2}\}) \\
L_{12} &= (A^2/4)\{1 - [p/(1+p^2)^{1/2}]\} \\
&\quad \times (1 - \{(p+N)/[1+(p+N)^2]^{1/2}\}) \\
L_{21} &= (A^2/4)\{1 + [p/(1+p^2)^{1/2}]\} \\
&\quad \times (1 + \{(p+N)/[1+(p+N)^2]^{1/2}\}).
\end{aligned} \tag{16}$$

Again, $L_{11} + L_{22} + L_{12} + L_{21} = A^2$.

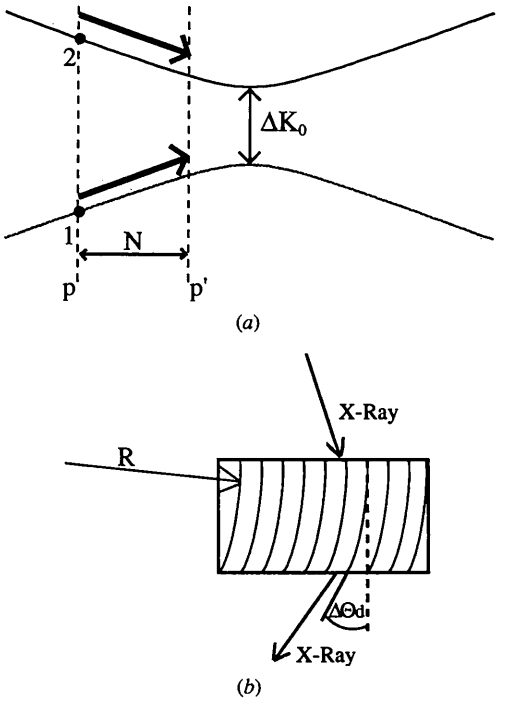

Fig. 3. (*a*) X-ray dispersion surface with movable tie points 1 and 2 for a cylindrically bent crystal [(*b*)].

In the case of a small strain gradient satisfying the condition (Authier & Balibar, 1970)

$$|\mathbf{b}|\tau/2\pi < \Delta K_o/H \quad \text{or} \quad B < 1, \tag{17}$$

where B is a dimensionless strain gradient defined as

$$B = |\mathbf{b}|H/\Delta K_o^2, \tag{18}$$

interbranch scattering processes without US are insignificant (Authier & Balibar, 1970; Balibar, Chukhovskii & Malgrange, 1983) [*i.e.*, again, in (11), coefficients $\alpha_{11} = \alpha_{22} = 1$, $\alpha_{12} = \alpha_{21} = 0$] and the diffraction profile $I_d(p)$ of a bent crystal is described analytically by a simple expression:

$$\begin{aligned}
I_d(p) &= L_{11} + L_{22} \\
&= (A^2/2)[1 - (p(p+N) \\
&\quad \times \{(1+p^2)[1+(p+N)^2]\}^{-1/2})].
\end{aligned} \tag{19}$$

The diffraction profile (19) is symmetric relative to the point $p_o = -N/2$ where the maximum in the diffraction spectrum is obtained. The maximum value of the diffraction intensity, $I_{\max}$, is given by

$$I_{\max} = I_d(p_o) = (A^2/2)(1 + \{(N^2/4)/[1 + (N^2/4)]\}) \tag{20}$$

and tends to $A^2 = 2I_o(0)$ [compare (6) and (20)] with an increase in N. At the points $p = 0$ and $p = -N$, the intensity $I_d = (A^2/2) = I_o(0)$. Thus, the effective width of the profile approximately equals N. The shapes of diffraction profiles $I_d(p)$ for several deformation parameters N are shown in Fig. 4. The behaviour of the integrated intensity $S(N) = \int I_d(p)\, dp$ is also important, since it can be compared with results obtained *via* the solution of the Takagi equations (Chukhovskii & Petrashen, 1977). The normalized dependence $S(N)/S(0)$ is shown in Fig. 5. In order to accord with

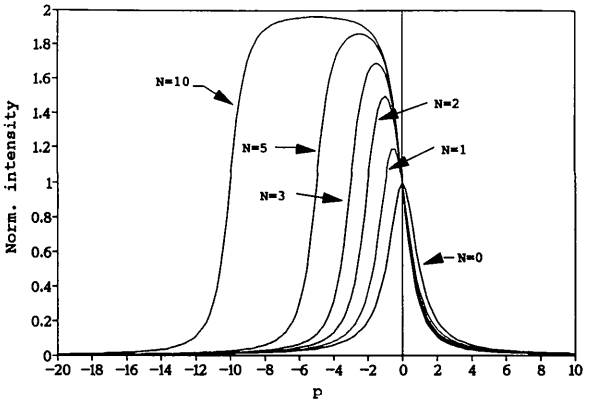

Fig. 4. Diffraction profiles $I_d(p)$ without US for several values of the deformation parameter N. The peak intensity of a perfect crystal is taken as 1.

well known results (Chukhovskii & Petrashen, 1977; Chukhovskii, 1980), the linear part of this plot should be described by the function

$$S(N)/S(0) = 4BT/\tau = 2N/\pi, \tag{21}$$

where the second equality is obtained by means of (15) and (18). In Fig. 6, the reduced data $\eta = N^{-1}S(N)/S(0)$ are plotted against N. This figure clearly demonstrates that, in fact, parameter η rapidly tends to a constant value of $2/\pi$ with an increase of N.

It can be concluded that, in the case of a constant strain gradient, a non-Lorentzian (rectangle-like, see Fig. 4) diffraction profile is formed that is N times broader than, and has almost twice the peak intensity of, a diffraction profile (Lorentzian) of a perfect crystal. Thus, the experimentally observed anomalous decrease in integrated intensity under a weak US excitation can be caused, in principle, by two mechanisms: narrowing of the diffraction profile or reduction of peak intensity. In §3, the effect of US on diffraction profiles is calculated directly.

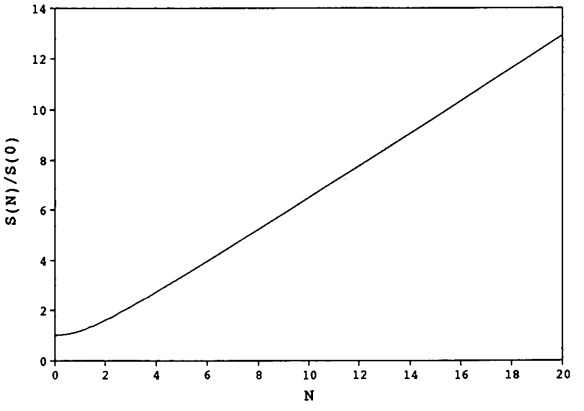

Fig. 5. The plot of normalized integrated diffraction intensity, $S(N)/S(0)$, as a function of deformation parameter N.

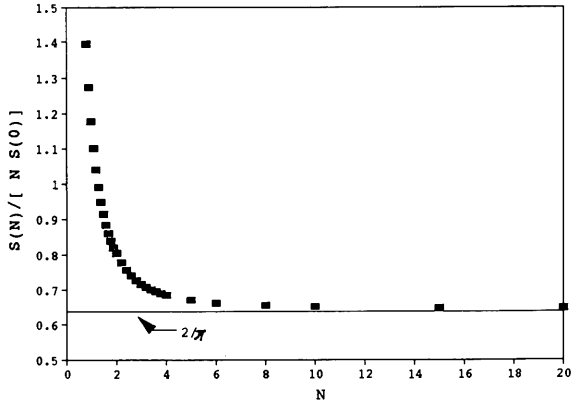

Fig. 6. The plot of reduced integrated intensity, $S(N)/[NS(0)]$, as a function of deformation parameter N, reaching asymptotically a limit of $2/\pi$.

3. X-ray diffraction profiles under ultrasound excitation

The approach developed can be extended to strained crystals undergoing US excitation. US stimulates X-ray inelastic scattering with emission and absorption of US phonons. Since the phonon energy is not comparable with the energy of X-ray quanta, only a wave-vector transfer should be considered. If the US wave vector **k** is directed along the reflecting planes ($\mathbf{k} \perp \mathbf{H}$) and $|\mathbf{k}| = k > \Delta K_o$ (high-frequency US), then in momentum space inelastic scattering processes are represented as interbranch jumps of tie points in the vicinity of definite positions $p_{\pm n}$ on the dispersion surface (interaction points). These points are located where the gap value $\Delta K = \Delta K_o(1 + p^2)^{1/2}$ equals an integer number $n = 1, 2, 3, \ldots$ of US wave vector k (see Fig. 7):

$$p_{\pm n} = \pm[(nk/\Delta K_o)^2 - 1]^{1/2}. \tag{22}$$

Interbranch transitions make the movement of tie points more complicated. As a result, cross terms L_{ij} in (11) should be taken into account. In principle, the 'fate' of every tie point must be followed because the contribution of a tie point to diffraction intensity will be different depending on its starting position p, the magnitude of the deformation parameter N and the positions p_n of essential multiphonon interaction points. In order to describe quantitatively the movement of tie points along the dispersion surface, two probabilities are introduced in each interaction point: R_n to remain on the same branch and M_n to jump to the other one ($R_n + M_n = 1$) because of the n-phonon process (Iolin, 1987; Iolin, Raitman, Kuvaldin & Zolotoyabko, 1988).

$$\begin{aligned} R_n &= \exp(-\pi F_n^2/2B) \\ F_n &= J_n(2Hw)[g^{-1/4}\delta_{n,2m+1} + g^{1/4}\delta_{n,2m}] \\ g &= 1 - [J_0(2Hw)\Delta K_o/nk)]^2, \end{aligned} \tag{23}$$

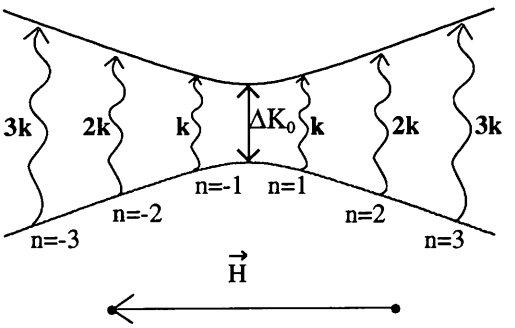

Fig. 7. Interaction points on the dispersion surface in a crystal undergoing high-frequency US excitation.

where $J_n(x)$ is a Bessel function of the nth order and δ_{ij} is the Kronecker delta. The number of US phonons that must be taken into account depends on the US amplitude w and can be evaluated using the asymptotes of these Bessel functions: the nth-order Bessel function, $J_n(x)$, becomes significant when its argument value $x \simeq n$. The diffraction profile will be described by (11), with L_{ij} functions (16) and the coefficients α_{ij} will be combinations of probabilities R_n and M_n.

The principle of calculation is illustrated by an example for $Hw < 1$, when only the one-phonon process is significant. With the removal of any ambiguity, $p_{\pm 1} = \pm 0.4$, $N = 2$ and a definite sign of strain gradient that provides a movement of tie points from left to right (see Fig. 8) are chosen. Under such conditions, the dispersion surface can be divided into several intervals of p values, where the US-induced modifications of the diffraction profile will be different.

(1) $-\infty < p < -2.4$. According to (14), the difference between starting and final p values is $\Delta p = N = 2$. It means that tie points in this range ($-\infty < p < -2.4$) will not be influenced by US, since they could not reach the left interaction point $p_{-1} = -0.4$ under the strain gradient (see Fig. 8*a*). The diffraction profile in this p range is still described by the same expression as without US:

$$I_d(p) = L_{11} + L_{22}. \tag{24}$$

(2) $-2.4 \le p < -1.6$. Tie points in this range will move under the strain gradient, reaching the left interaction point $p_{-1} = -0.4$ (see Fig. 8*b*). Thus, tie points will remain on the same branch with a probability R_1 and will jump to the other branch with probability M_1 ($R_1 + M_1 = 1$). Correspondingly, this part of the diffraction profile is expressed as

$$I_d(p) = R_1(L_{11} + L_{22}) + M_1(L_{12} + L_{21}). \tag{25}$$

(3) $-1.6 \le p \le -0.4$. The adiabatic movement of tie points is interrupted in both interaction points $p_{\pm 1} = \pm 0.4$ (see Fig. 8*c*). Therefore,

$$I_d(p) = (R_1^2 + M_1^2)(L_{11} + L_{22}) + 2R_1M_1(L_{12} + L_{21}). \tag{26}$$

(4) $-0.4 < p \le 0.4$. The situation is identical to that of case (2).

(5) $0.4 < p < \infty$. The situation is identical to that of case (1).

With (16) and (24)–(26), diffraction profiles can be simulated at different US amplitudes, *i.e.* at different R_1 values; several examples are shown in Fig. 9. The results obtained show a cancellation of the strain-induced excess of diffraction intensity in the vicinity of the profile maximum, rather than a narrowing of the diffraction profile.

In order to obtain more detailed data in the wider w range, simulations were performed of diffraction profiles in the three-phonon approximation ($p_{\pm 1} = \pm 0.4$, $p_{\pm 2} = \pm 1.9$, $p_{\pm 3} = 3.0$) up to $2Hw = 2$. All possible trajectories of tie points were taken into account. The integrated diffraction intensities for $N = 1, 2, 3$

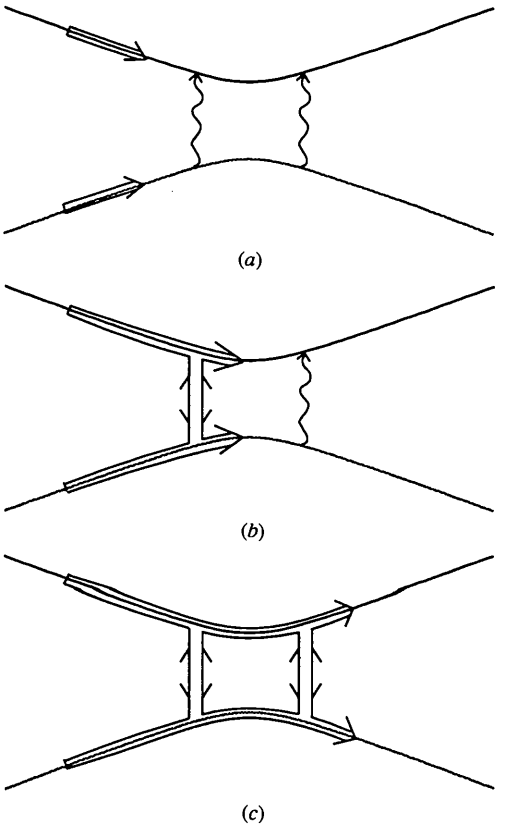

Fig. 8. Possible trajectories of tie points in reciprocal space under one-phonon US excitation. Details of (*a*), (*b*) and (*c*) are given in the text.

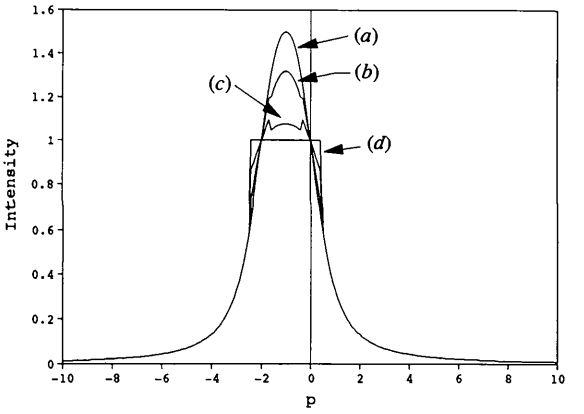

Fig. 9. Diffraction profiles for $N = 2$, calculated in the one-phonon approximation at different US amplitudes, corresponding to several R_1 values: (*a*) 1.0; (*b*) 0.9; (*c*) 0.7; (*d*) 0.5. The peak intensity for a perfect crystal was taken as 1.

($B = 0.1$) depending on US amplitude are shown in Fig. 10. The anomalous decrease in integrated intensity at small Hw becomes more pronounced with an increase in the deformation parameter N, which agrees well with experimental data (Iolin, Raitman, Kuvaldin & Zolotoyabko, 1988; Zolotoyabko & Panov, 1992). This decrease is due to a reduction in peak intensity without profile narrowing, as is clearly seen again in Fig. 11, where several profiles at $N = 3$ and $x = 2Hw < 1$ are shown. With a further increase in the US amplitude, a growth in integrated intensity is observed (Fig. 10), which is a result of satellite formation. The satellite-like structure of the diffraction profiles is clearly revealed at $x = 2Hw \geq 1$ (see Fig. 12). It should be noted that, although the diffraction spectra of strained crystals are undoubtedly coupled with the satellite positions in a perfect crystal ($p_{\pm n}$ points), the profiles in Fig. 12 are more complicated. The observed features are mostly determined by the number of regions on the dispersion surface that are nonequivalent in the sense of the topology of tie-point trajectories.

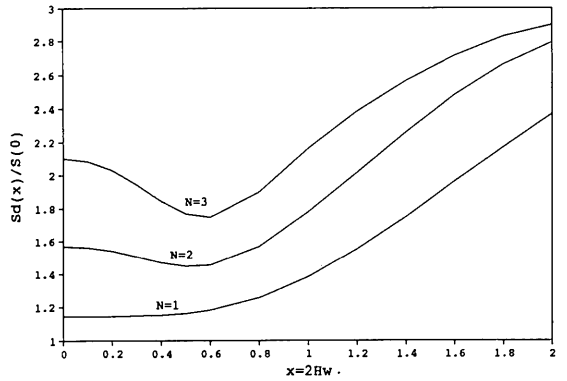

Fig. 10. Integrated diffraction intensities for $N = 1$, 2 and 3 depending on US amplitude. Three-phonon approximation.

4. Concluding remarks

The approach developed allows the description of the modifications in diffraction profiles (Laue case) evolving in elastically bent crystals without, as well as with, US excitation. Diffraction profiles $I_d(p)$ without US (19) tend to have a rectangle-like shape with a maximum intensity $I_{max} \simeq 2I_o(0)$ and a width $\Gamma_d \simeq N$ as the deformation parameter N increases (see Fig. 4). Thus, the diffraction profile I_d is much broader than for an ideal crystal ($\Gamma_d > \Gamma_o = 2$) and has nearly twice the peak intensity. A comparison between the integrated intensity for such a profile, $S_d \simeq I_{max}\Gamma_d \simeq 2I_o(0)N$, and the area under a Lorentzian (6) for an ideal crystal, $S_o = \pi I_o(0)\Gamma_o/2 = \pi I_o(0)$, leads to a ratio $S_d/S_o = 2N/\pi$, which can be considered as a large-N asymptote. It coincides with results obtained using Takagi equations in the case of small strain gradients ($B < 1$), when the interbranch scattering processes can be neglected.

High-frequency US creates a new channel of interaction between the branches of the dispersion surface. Inelastic X-ray scattering on an acoustic superlattice provides an independent jumping mechanism for tie points, with the jumping probability increasing rapidly with the growth of US amplitude. Correspondingly, a redistribution of X-ray quanta between transmitted and diffracted beams occurs. As a result, the anomalous dependence of the integrated intensity is observed, with a dip formation at small US amplitudes. In the beginning, the dip value ξ increases with N (see Fig. 10). Experimental data show, however, that ξ never exceeds 50% (Iolin, Raitman, Kulvaldin & Zolotoyabko, 1988; Zolotoyabko & Panov, 1992). Calculations have demon-

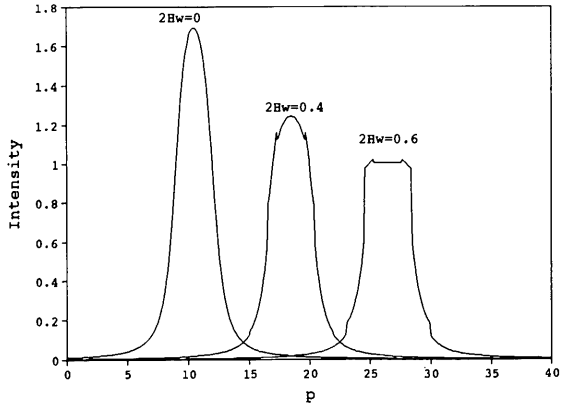

Fig. 11. Diffraction profiles in a strained crystal undergoing US excitation. Three-phonon approximation. $N = 3$, $x = 2Hw < 1$. The curves are artificially shifted from the origin for a better resolution of their shape.

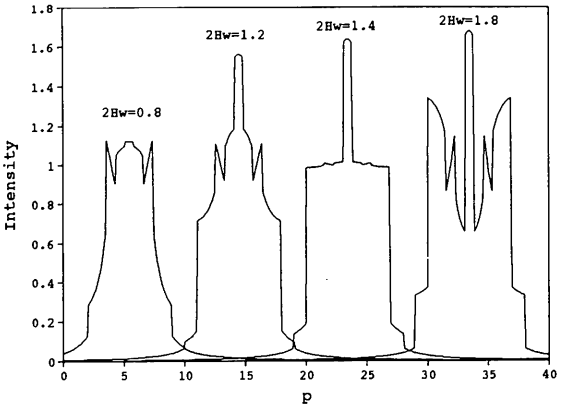

Fig. 12. Diffraction profiles in a strained crystal undergoing US excitation. Three-phonon approximation. $N = 3$, $x = 2Hw \geq 1$. The curves are artificially shifted from the origin for a better resolution of their shape.

strated that the dip formation is not related to a narrowing of the diffraction profile but rather is caused by a decrease in peak intensity (see Fig. 9). The reduction of the strain-induced excess of peak intensity takes place from I_{max} [see (20)] to the level of a perfect crystal, $I_{min} = I_o(0) = A^2/2$ [see (6)]. With the quasirectangular shape of the diffraction profiles taken into account, the dip value ξ in integrated intensity can be estimated *via* the variation in peak intensities (at least in the limit of large N):

$$\xi = (I_{max} - I_{min})/I_{max} = (N/2)^2/[1 + 2(N/2)^2]. \quad (27)$$

From (27) follows a growth in the dip magnitude with an increase in N up to $\xi = 0.5$, in agreement with experimental data. Note that, for $N \leq 5$, (27) will provide somewhat overestimated ξ values owing to deviation of diffraction profiles from a rectangle-like shape.

It was shown (Iolin, Raitman, Kuvaldin & Zolotoyabko, 1988) that the reduction in the integrated intensity due to interbranch jumping is maximum for $Hw \simeq B^{1/2}$. Thus, in our case of $B = 0.1$, $2Hw \simeq 0.6$ coincides with the dip position on the curves in Fig. 10. When the US amplitude is raised, the multiphonon scattering processes become significant, and a broadening in diffraction profiles occurs because of satellite formation (see Fig. 12) that leads to an increase in integrated intensity (see Fig. 10). The structure of diffraction profiles depends on different parameters (N, B, $k/\Delta K_o$, w) and reveals interesting features. For example, an extremely narrow rectangle-like component is observed in Fig. 12 (at $2Hw = 1.4$), having a full width $\Gamma \simeq 0.3\Gamma_o$. Such components may be used, in principle, in monochromatization systems for synchrotron radiation.

Note that detailed measurements of diffraction profiles under ultrasonic excitation have not been performed even in perfect crystals, not to mention strained ones. Few experimental observations of ultrasonically induced diffraction satellites [see, for example, Entin & Assur (1981) and Chapman, Colella & Bray (1983) have been made in the Bragg scattering geometry. These experiments demonstrated only in principle the appearance of satellites, without focusing on the strain state of the sample. The main efforts were aimed at easier measurements of integrated diffraction intensity. Thus, the amazing graphs in Fig. 12 may be considered a challenge to X-ray groups having double-crystal diffractometers with angular accuracy of the order of 0.1″.

The last remark concerns the important narrowing effect of rocking curves at small US amplitudes (with approximately the same peak intensity) that was experimentally obtained in the Bragg case (Zolotoyabko, Sander, Komem & Kantor, 1993, 1994). It can be concluded that, apparently, it is a specific effect for a given scattering geometry. In fact, in the Bragg case, the reflection coefficient in the range of total reflection equals 1 for a perfect crystal. Thus, the growth of integrated intensity under strain gradient (see, for example, Uschmann, Forster, Gabel, Holzer & Ensslen, 1993) must be related to a broadening in the diffraction profile alone. Correspondingly, the reverse process – the US-induced redistribution of X-ray quanta (restoration of diffraction profile to an ideal shape) at small US amplitudes – should first of all lead to a narrowing of the diffraction spectrum as a result of the limited degree of freedom in the peak intensity variation. This problem is now under investigation and the results will be published in a separate paper.

This work was supported by the Israel Ministry of Science and Technology and Schlesinger Fund (grant no. 040-515). It was also partly supported by the Jewish Communities of Germany Research Fund (grant no. 040-552) and by Technion V.P.R. Fund – P. and E. Nathan Research Fund (grant no. 040-498). One of the authors (EZ) would also like to thank the Fund for the Promotion of Research at the Technion.

References

ANDREEV, A. V., PONOMAREV, YU. V. & SMOLIN, A. A. (1988). *Sov. Tech. Phys. Lett. (Engl. Transl.)*, **14**, 550–552.
AUTHIER, A. & BALIBAR, F. (1970). *Acta Cryst.* A**26**, 647–654.
BALIBAR, F., CHUKHOVSKII, F. & MALGRANGE, C. (1983). *Acta Cryst.* A**39**, 387–399.
BONSE, U. (1964). *Z. Phys.* **177**, 385–423, 529–542, 543–561.
CERVA, H. & GRAFF, W. (1984). *Phys. Status Solidi A*, **82**, 35–45.
CHAPMAN, L. D., COLELLA, R. & BRAY, B. (1983). *Phys. Rev. B*, **27**, 2264–2277.
CHUKHOVSKII, F. N. (1980). *Metallofizika.* **2**, 3–27.
CHUKHOVSKII, F., NOSIK, V. & IOLIN, E. (1993). *Sov. Phys. JETP (Engl. Transl.)*, **77**, 102–112.
CHUKHOVSKII, F. N. & PETRASHEN, P. V. (1977). *Acta Cryst.* A**33**, 311–319.
ENTIN, I. (1977). *Sov. Phys. JETP Lett. (Engl. Transl.)*, **26**, 269–271.
ENTIN, I. (1979). *Sov. Phys. JETP (Engl. Transl.)*, **50**, 110–113.
ENTIN, I. & ASSUR. K. (1981). *Acta Cryst.* A**37**, 769–774.
ENTIN, I., KHRUPA, V. & DATSENKO, L. (1990). *J. Appl. Cryst.* **23**, 355–358.
HART, M. (1980). In *Characterization of Crystal Growth Defects by X-ray Methods*, edited by B. K. TANNER & D. K. BOWEN. New York/London: Plenum Press.
IOLIN, E. (1987). Preprint LAFI-102. Physics Institute of the Latvian Academy of Science, Salaspils, Latvia.
IOLIN, E., RAITMAN, E., KUVALDIN, B. & ZOLOTOYABKO, E. (1988). *Sov. Phys. JETP (Engl. Transl.)*, **67**, 989–997.
KATO, N. (1963). *J. Phys. Soc. Jpn*, **18**, 1785–1791.
KATO, N. (1964). *J. Phys. Soc. Jpn*, **19**, 67–77.
KHRUPA, V., ENTIN, I. & DATSENKO, L. (1991). *Phys. Status Solidi A*, **125**, 451–457.
KIKUTA, S., TAKAHASHI, T. & NAKATANI, S. (1984). *Jpn. J. Appl. Phys.* **23**, L193–L194.
KOCHARYAN, L. A., SUKIASYAN, R. R., MEGRABYAN, KH. S. & SARKISYAN, T. V. (1989). *Sov. Tech. Phys. Lett. (Engl. Transl.)*, **15**, 377–378.
KOHLER, R., MOHLING, W. & PEIBST, H. (1974). *Phys. Status Solidi B*, **61**, 173–180.
PENNING, P. (1966). *Philips Res. Rep.* **21**, 1–109.

PENNING, P. & POLDER, D. (1961). *Philips Res. Rep.* **16**, 419–440.
PINSKER, Z. G. (1978). *Dynamical Scattering of X-rays in Crystals*. Berlin: Springer-Verlag.
RARANSKII, N., FODCHUK, I., NOVIKOV, S. & KOROVYANKO, O. (1993). *Metallofizika*, **15**, 85–91.
ROSHCHUPKIN, D. V., BRUNEL, M., BERGEVIN, F. D. & ERKO, A. I. (1992). *Nucl. Instrum. Methods Phys. Res. B*, **72**, 471–476.
TAKAGI, S. (1962). *Acta Cryst.* **15**, 1311–1312.
TAKAGI, S. (1969). *J. Phys. Soc. Jpn*, **26**, 1239–1253.
USCHMANN, I., FORSTER, E., GABEL, K., HOLZER, G. & ENSSLEN, M. (1993). *J. Appl. Cryst.* **26**, 405–412.
ZOLOTOYABKO, E., JACOBSOHN, E., SHECHTMAN, D., KANTOR, B. & SALZMAN, J. (1993). *J. Appl. Phys.* **73**, 8647–8649.
ZOLOTOYABKO, E. & PANOV, V. (1992). *Acta Cryst.* A**48**, 225–231.
ZOLOTOYABKO, E., PANOV, V. & SCHVARKOV, D. (1993). *Rev. Sci. Instrum.* **64**, 1274–1279.
ZOLOTOYABKO, E., POLIKARPOV, I., PANOV, V. & SCHVARKOV, D. (1992). *J. Appl. Cryst.* **25**, 88–91.
ZOLOTOYABKO, E., SANDER, B., KOMEM, Y. & KANTOR, B. (1993). *Appl. Phys. Lett.* **63**, 1540–1542.
ZOLOTOYABKO, E., SANDER, B., KOMEM, Y. & KANTOR, B. (1994). *Acta Cryst.* A**50**, 253–257.

Acta Cryst. (1995). A**51**, 171–177

Accurate Elastic Scattering Factors for Lithium to Argon Based on Correlated Wavefunctions

BY HERMANN MEYER, THOMAS MÜLLER AND ARMIN SCHWEIG*

Fachbereich Physikalische Chemie und Zentrum für Materialwissenschaften, Universität Marburg, Postfach, D-35032 Marburg, Germany

(*Received* 16 *May* 1994; *accepted* 28 *August* 1994)

Abstract

Elastic scattering factors (or atomic form factors) $f(s)$ for Li to Ar have been derived in the first Born approximation from *ab initio* MR-SDCI (multireference singly and doubly excited configuration interaction) calculations which recover between 90 and 99% of the estimated total correlation energy. The correlation effects on $f(s)$ are contrasted with the relativistic effects known from the literature. Atomic form factors are presented that take into account correlation and relativistic contributions in an additive manner.

Introduction

Elastic scattering factors (or atomic form factors) $f(s)$ listed in *International Tables for Crystallography* (Maslen, Fox & O'Keefe, 1992) are widely used in crystallographic structure calculations. Except for hydrogen, they were computed from relativistic Dirac–Fock wavefunctions which completely neglect electron correlation. However, at least for light atoms, correlation effects are expected to be more significant than relativistic corrections. For two-electron systems and, restricted to rather few s values, for Li and Be, accurate atomic form factors are available that account for more than 99% of the estimated total correlation energy (Thakkar & Smith, 1992; Schmider, Esquivel, Sagar & Smith, 1993; Esquivel & Bunge, 1987). For B to Ne, atomic form factors including correlation contributions were published but they either do not account for a sufficient amount of electron correlation (Tanaka & Sasaki, 1971; Peixoto, Bunge & Bonham, 1969) or they rely on non-variational configuration interaction schemes (Naon & Cornille, 1973). For Na to Ar, no correlation calculations of form factors have been published to date. In the present work, atomic form factors are derived based on *ab initio* MR-SDCI (multireference singly and doubly excited configuration interaction) calculations which recover between 90 and 99% of the estimated total correlation energy. The resulting correlation contributions to $f(s)$ are compared with corresponding relativistic contributions known from the literature.

* To whom correspondence should be addressed.

Computational details

The atomic form factor in the framework of the first Born approximation (Waller & Hartree, 1929) is given by

$$f(\mathbf{s}) = \int \rho(\mathbf{r}) \exp(i\mathbf{sr}) d\mathbf{r}, \quad (1)$$

where $\mathbf{r}$ denotes the position vector of an electron, $\rho(\mathbf{r})$ the one-electron density and $\mathbf{s}$ the scattering vector. The magnitude of $\mathbf{s}$ is the scattering variable s which depends on the wavelength λ of the radiation and the scattering angle 2θ according to $s = (4\pi/\lambda)\sin\theta$. If the one-electron density is expanded in terms of GTOs (Gaussian-type orbitals), χ_μ, the spherically averaged form factor is obtained as

$$f(s) = (1/4\pi)\int f(\mathbf{s}) d\Omega$$
$$= (1/4\pi)\sum_{\mu\nu} P_{\mu\nu} \int\int \chi_\mu(\mathbf{r})\chi_\nu(\mathbf{r}) \exp(i\mathbf{sr}) d\mathbf{r} d\Omega, \quad (2)$$